Optical and structural properties of cadmium telluride films grown by glancing angle deposition

2013 Phys. Scr. 88 025602

(http://iopscience.iop.org/1402-4896/88/2/025602)

Phys. Scr. **88** (2013) 025602 (7pp) doi:10.1088/0031-8949/88/02/025602

Optical and structural properties of cadmium telluride films grown by glancing angle deposition

M H Ehsani, H Rezagholipour Dizaji, S Azizi, S F Ghavami Mirmahalle and F Hosseini Siyanaki

Thin Film Laboratory, Faculty of Physics, Semnan University, Semnan, Iran

E-mail: hrgholipour@semnan.ac.ir

Received 24 February 2013
Accepted for publication 10 June 2013
Published 9 July 2013
Online at stacks.iop.org/PhysScr/88/025602

Abstract

Cadmium telluride films were grown by the glancing angle deposition (GLAD) technique. The samples were prepared under different incident deposition flux angles ($\alpha = 0^\circ$, 20° and 70° measured from the normal to the substrate surface). During deposition, the substrate temperature was maintained at room temperature. The structural study was performed using an x-ray diffraction diffractometer. The samples were found to be poly-crystalline with cubic structure for those deposited at $\alpha = 0^\circ$ and 20° and hexagonal structure for the one deposited at 70°. The images of samples obtained by the field emission scanning electron microscopy technique showed that the GLAD method could produce a columnar layer tilted toward the incident deposition flux. The optical properties study by the UV–Vis spectroscopy technique showed that the use of this growth technique affected the optical properties of the films. A higher absorption coefficient in the visible and near-IR spectral range was observed for the sample deposited at $\alpha = 70^\circ$. This is an important result from the photovoltaic applications point of view where absorber materials with large absorption coefficients are needed. Also, it seems that the sample with a high incident deposition flux angle has the capability of making an n-CdTe/p-CdTe homo-junction.

PACS numbers: 68.55.−a, 81.15.Aa, 78.20.−e

(Some figures may appear in color only in the online journal)

1. Introduction

The first investigations on physical vapor deposition (PVD) of thin films showed that the micro- and nano-structures of deposited coatings were strongly influenced by operating conditions such as vapor pressure, deposition rate, substrate temperature, film thickness and ion-to-atom incident ratio [1–4]. The formation of a typical columnar microstructure through application of high pressure and low substrate temperature was reported by Thornton [1].

The glancing angle deposition (GLAD) technique is a technique capable of engineering the columnar structure of thin films on an ordered array of micro- and nanoscale [5, 6]. It was first reported in 1959 by Knorr and Hoffman [7]. In the PVD technique the vapor flux, consisting of atoms and molecules from the gas phase, is commonly parallel to the substrate normal, while in the GLAD method the vapor flux arrives at the substrate surface at an oblique angle (α) that is measured from the normal to the substrate surface, as shown in figure 1. During the GLAD process, the tilted columns form on the substrate due to the atomic-scale shadowing (so-called 'self-shadowing') effect. In fact, during deposition at an oblique angle, the evaporant does not nucleate at the region that falls in the 'shadow' of the nucleus, as can be seen in figure 1. Therefore, the vapor will only deposit onto the nuclei keeping the growth in the oblique angle direction, which means that the shadowing effect guarantees the formation of slanted columnar structure.

Under oblique angle deposition, the columns will continue to grow in the tilted direction with an angle β that is usually smaller than the angle α, as shown in figure 1.

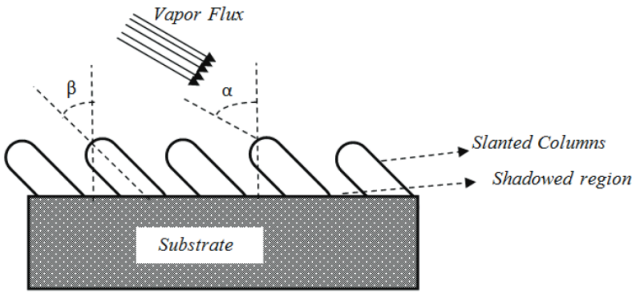

Figure 1. Sketch showing the GLAD process.

The relation between the column angle (β) and the flux angle (α) is given by Driks and Leamy [8]:

$$\tan\,\beta = \frac{1}{2}\tan\,\alpha. \tag{1}$$

Another relation suggested by Tait *et al* [9] is represented as the following:

$$\beta = \alpha - \sin^{-1}\left(\frac{1-\cos\alpha}{2}\right). \tag{2}$$

Both the relations have been used for GLAD deposited films by Xiao *et al*; however, they found that the latter one is more accurate for larger values of α ($>50^\circ$) [10]. It may be noted that the substrates are typically held at an oblique angle with respect to the vertical axis, as shown in figure 2, and remain stationary during the deposition. The development of the GLAD technique by rotating the substrate could alter the apparent location of the vapor source from the perspective of the growing columns [11]. So, in this process, there is a dynamic shadowing effect and the columns growth can therefore be sculpted by dynamic rotation of the substrate. This development can create a wide variety of morphologies (inclined columns, straight pillars, helix, zigzag shapes) with a change in direction of the incident flux and rotation rate of the substrate [5, 6, 11]. This technique has been used for the fabrication of thin films with applications in the area of sensing technologies, optical devices including polarizers, high birefringence biaxial films, spectral hole filters, nano-emitters, etc [12–16].

In recent years, polycrystalline CdTe materials have been considered to be very suitable for the fabrication of solar cells due to their direct band gap and high absorption coefficient [17]. Also, it has been reported that the GLAD technique can affect the optical parameters of other semiconductor films [10, 18–21]. As reported recently, obliquely CdTe deposited films show a much higher photovoltage magnitude than the band gap [20, 22]. It may be attributed either to the mismatch between adjacent hillocks produced by the self-shadowing effect or to the transition between cubic and hexagonal structures as described by Dhere *et al* [23].

The present investigation is mainly focused on the optical properties of CdTe films deposited at an oblique angle, which has not been elaborately studied by the others to the best of our knowledge. For this purpose, we used the GLAD technique with a little variation from the conventional technique in our coating machine (Hind-HiVac coating unit (Model-15F6)) as described below.

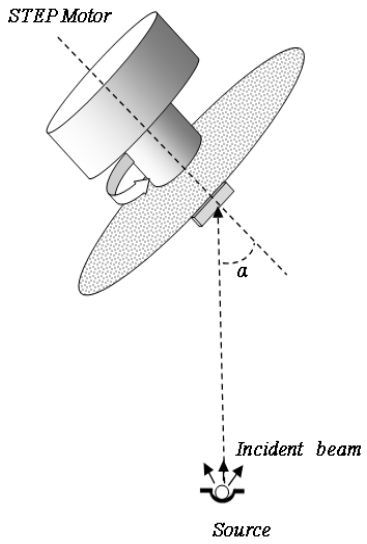

Figure 2. Sketch showing the usual system of GLAD (tilted and rotated substrate).

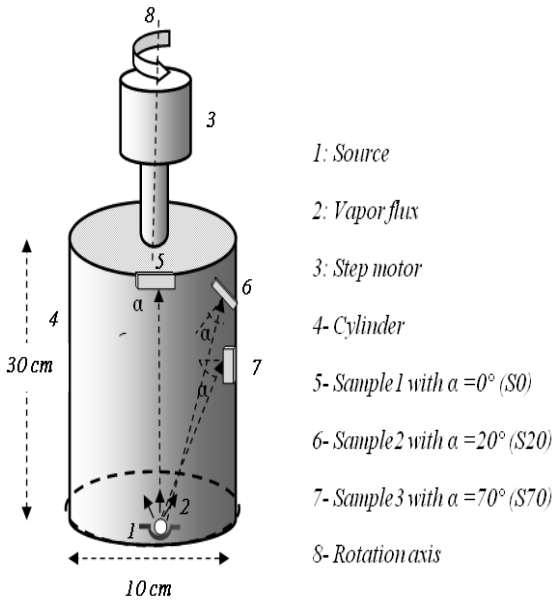

Figure 3. Schematic showing the relative position of source and rotating substrate.

As illustrated in figure 3, the mechanism of substrate rotation is angular rotation rather than spinning rotation as in the case of the conventional GLAD technique (figure 2). Some capabilities and advantages of this system have been described by the authors elsewhere [24]. Briefly, the cylinder bottom is open to allow the vapor flux transferring from the source to the substrates and it acts like a quasi-closed space for vapor flux. The substrate can be fixed on the inner wall as well as on the upper surface of the cylinder. The rotation of the cylinder was done by a step motor coupled to it. Therefore, during a complete cylinder rotation, the substrate rotates about the cylinder axis.

Using the above-mentioned equipment, three CdTe samples under different conditions were prepared and studied using x-ray diffraction (XRD) (ADVANCE–D8 model), UV–Vis spectrophotometry (Shimadzu Model UV-1650 PC)

and field emission scanning electron microscopy (FESEM) techniques (Hitachi, Model S-4160).

2. Experimental procedure

CdTe films were deposited onto glass substrates in a Hind-HiVac coating unit (Model-15F6). The substrates were cleaned in acetone using an ultrasonic bath and then dried with purified nitrogen gas. Further, the substrates were subjected to glow discharge cleaning before deposition. The base pressure of the chamber was 5×10^{-6} mbar. CdTe powder of 99.99% purity supplied by Aldrich Company was evaporated from a molybdenum boat. The deposition rate was measured and controlled *in situ*, for a non-angled rotating substrate, by using a Hind-HiVac thickness monitor (Model DTM-101). The average typical growth rate was 10 Å s^{-1}. The film thickness was verified by the cross-sectional image provided by FESEM.

In order to investigate the effect of variation in incident flux on the optical and structural properties of CdTe films during deposition, three types of specimens were produced under different conditions. They were labeled as S0, S20 and S70 where the digits 0, 20 and 70 correspondingly refer to the angle with respect to the normal of the substrate surface at which the substrates have been fixed inside the cylinder. During the deposition processes, the cylinder was rotated at 50 rpm by applying a suitable dc voltage to the step motor.

To produce a slanted columnar structure on each substrate, all the three substrates were fixed at the above-mentioned condition (figure 3) and deposition was carried out simultaneously. After depositing the first layer, the substrates were removed from the coating chamber and rotated 180° about their normal axis and then the deposition of the second layer was performed. Finally, the films were removed from the coating chamber and exposed to the ambient atmosphere. The x-ray pattern of the specimens was used to study the structure of CdTe films. The optical properties of the specimens were investigated using the data collected from transmission and reflection spectra provided by the UV–Vis spectrophotometer. The top and cross-sectional images of the specimens were obtained using FESEM.

3. Results and discussion

3.1. Structural characteristics

The XRD patterns of samples S0, S20 and S70 are shown in figures 4–6, respectively. In figures 4–5 the diffraction peaks observed at $2\theta = 23.58°$, 39.1°, 46.7° and 76.2° are due to reflections from the (111), (220), (311) and (511) CdTe crystallographic planes in the cubic structure with the *F*-4-3*m* space group and $a = b = c = 6.48$ Å. The presence of a peak at $2\theta = 21.4°$ is attributed to the Te element, which indicates that both the samples are Te rich [23, 25]. The intensity of all the peaks, especially the main peak due to the (111) CdTe plane, decreases with increasing incident angle α. It is more significant in the case of sample S70, as can be observed in figure 6. In addition, sample S70 experiences a phase transition from cubic to hexagonal. It is a general characteristic of the GLAD technique to produce obliquely deposited films with poor crystallinity and sometimes amorphous structure [18, 19, 26]. The reason for this is attributed to the shadowing effect, which limits ad-atom

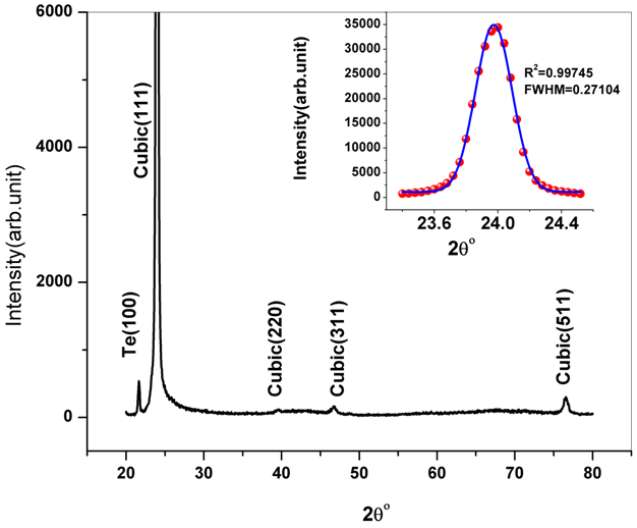

Figure 4. XRD pattern of the S0 sample. The top right corner shows the Gaussian fitting for the main peak.

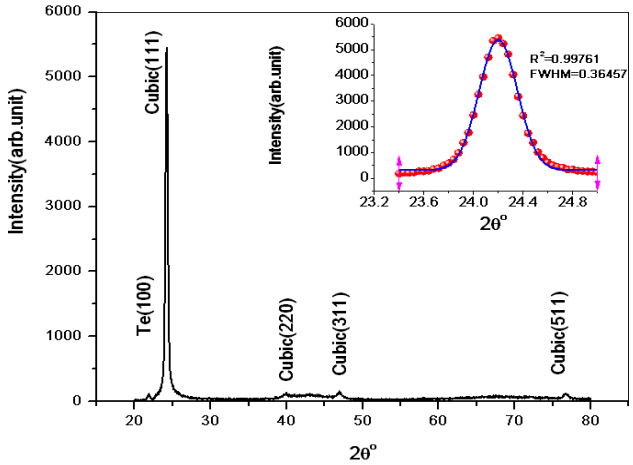

Figure 5. XRD pattern of the S20 sample. The top right corner shows the Gaussian fitting for the main peak.

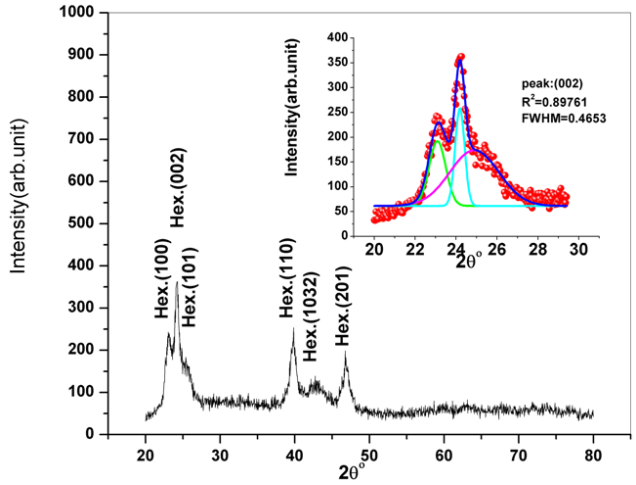

Figure 6. XRD pattern of the S70 sample. The top right corner shows the Gaussian fitting for the three main peaks.

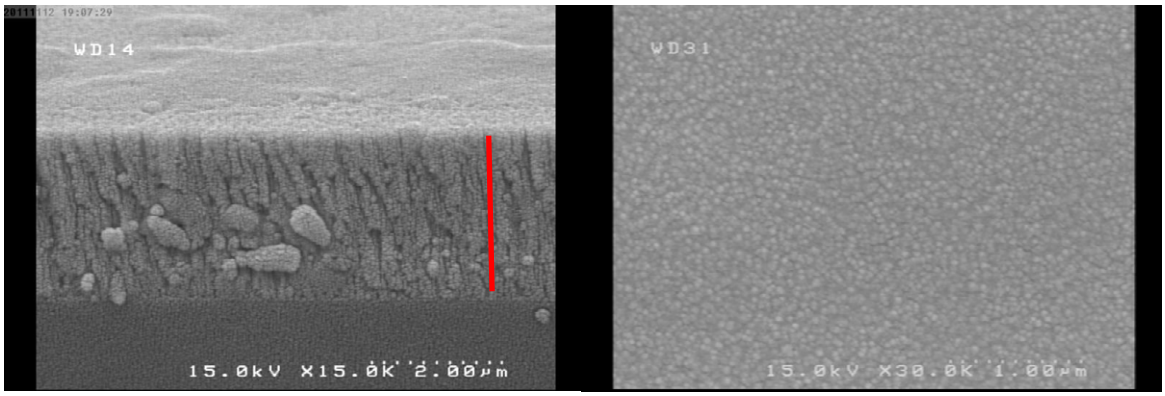

Figure 7. Top view (left) and cross-sectional (right) FESEM images of sample S0.

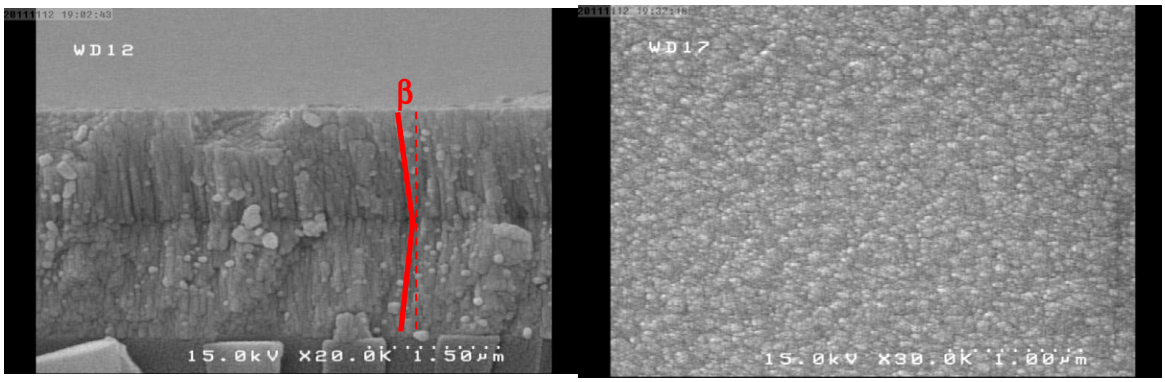

Figure 8. Top view (left) and cross-sectional (right) FESEM images of sample S20.

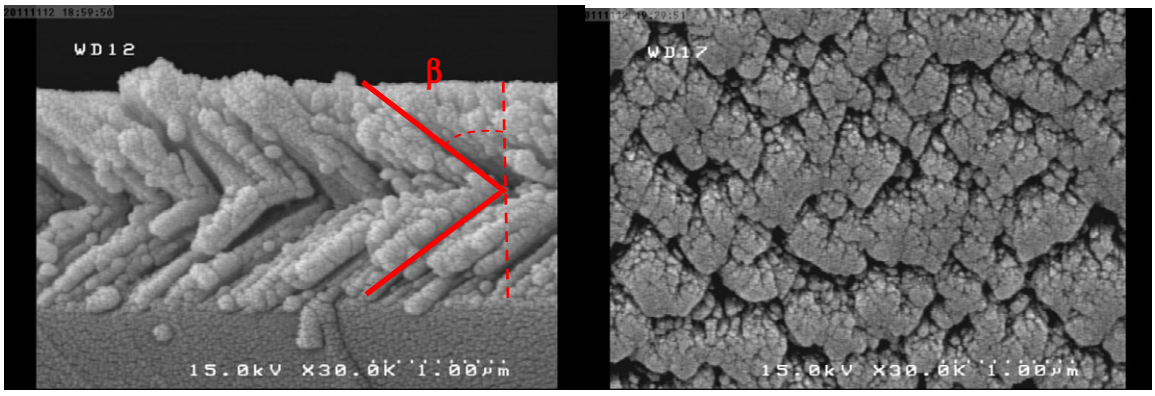

Figure 9. Top view (left) and cross-sectional (right) FESEM images of sample S70.

diffusion at room temperature [5, 6]. The diffraction peaks observed in the XRD pattern of S70 are at $2\theta = 22.88^\circ$, 24.12°, 25.34°, 39.83°, 42.8° and 46.77° corresponding, respectively, to (100), (002), (101), (110), (103) and (201) CdTe crystallographic planes in hexagonal structure with the *P*63*mc* space group and lattice constants of $a = b = 4.58$ Å and $c = 7.5$ Å. A meaningful difference between the XRD pattern of S70 with those of S0 and S20 is the disappearance of the peak due to the Te element in it. It is known that the hexagonal and cubic phases are formed due to a deviation from stoichiometry, the cubic phase being favored by an excess of Te and the hexagonal phase being favored by an excess of Cd [27]. Also it is well understood that CdTe exhibits n-type or p-type features depending on whether it is rich in Te or Cd, respectively [28]. Thus, by applying a change in incident angle of vapor flux toward the substrate surface during the deposition process, there is the possibility of constructing an n-CdTe/p-CdTe homo-junction structure.

The Gaussian fitting for the main peaks of all the samples, shown at the top right corner in figures 4–6, was carried out. The grain size estimated by Scherrer's formula was found to be 30.16, 22.51 and 17.50 nm for samples S0, S20 and S70, respectively.

The surface and cross-sectional images of samples S0, S20 and S70, obtained by FESEM, are shown in figures 7–9, respectively. These images show the formation of L-shaped-like slanted columnar structure for the S20 and S70 samples. Using the side images obtained by FESEM, the films' thickness was estimated to be about 3, 3 and 2 μm for samples S0, S20 and S70, respectively. As expected, by

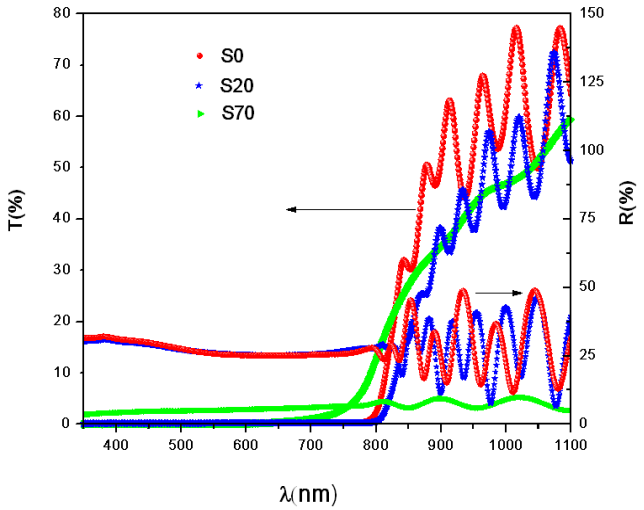

Figure 10. CdTe film transmittance and reflectance spectra of samples S0, S20 and S70.

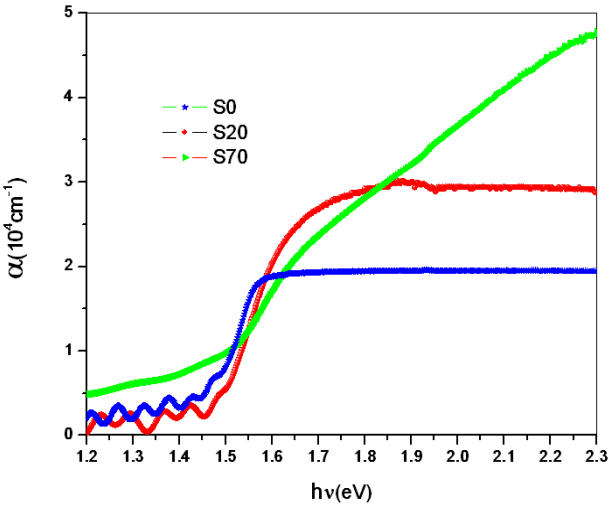

Figure 11. Absorption coefficient versus $h\upsilon$ (photon energy) for samples S0, S20 and S70.

increasing the vapor flux angle, the shadowing geometry and low ad-atom mobility on the film surface cause the appearance of nanostructure with large porosity in the case of the S70 sample (see figure 9 (right)). Hence, the most significant characteristic of oblique deposition is the creation of porous films. The density of films produced by the GLAD technique is given by the following formula [11]:

$$\frac{\rho}{\rho_0} = \frac{2\cos\alpha}{1+\cos\alpha}, \tag{3}$$

where ρ_0 and ρ are the densities of the films deposited at incident angle α equal to zero and non-zero, respectively. A simple calculation shows that the film density ratio of sample S70 to sample S0 is nearly $1/2$. This is an indication of the effect of oblique deposition on the nature of the film surface.

As one can obviously observe from figure 9 (left), the columns are not isolated completely and the film seems to be almost continuous. Due to the rotation of substrate, a dynamic shadowing effect occurs as reported by others [5, 6, 11]. Thus, it causes an increase in the column number density value. Therefore, it seems that the employed system is useful when one wants to produce films with nanostructure columns accompanied by high column number density. Using equations (1) and (2) the slanted column angles of samples S20 and S70 were calculated and found to be approximately 10.31° and 50.79°, respectively. The column angles measured using the cross-sectional images of samples S20 and S70 were found to be $\beta \approx 10°$ and $\approx 50°$, which shows good agreement with the calculated values.

3.2. Optical studies

The transmittance (T) and reflectance (R) spectra of the samples are presented in figure 10. The spectra exhibit interference behavior with a sharp fall in transmittance at the band gap, which is an indication of good crystallinity of the prepared specimens. The origin of this oscillating behavior is the formation of constructive and destructive wave interferences, which has been frequently reported by others [29–32].

It is observed from the figure that the transmittance of sample S70 has decreased and its oscillating behavior has been suppressed. The same observation has been reported for obliquely deposited $CuInS_2$ [19, 21], ZrO_2 [20], SnO_2:Sb [10] and Nb_2O_5 [18] films.

Figure 11 gives the graph of the absorption coefficient (α) versus photon energy ($h\upsilon$) for the three specimens. The absorption coefficient of a layer with thickness d, above the fundamental band edge, is given by the following equation [33]:

$$\alpha = \left(\frac{1}{d}\right) \mathrm{Ln}\left(\frac{(1-R)^2}{T}\right). \tag{4}$$

The absorption coefficient of sample S70 was found to be higher than that of the other two specimens in the visible and near-IR spectral ranges.

This interesting result may be related to the phase transition and appearance of the hexagonal phase in the case of S70 which has nanostructure.

Also we noticed that employing the GLAD technique affected the band gap of specimens. The following equation was used to calculate the specimens' energy band gap [34]:

$$(\alpha h\upsilon)^2 = A\left(h\upsilon - E_g\right), \tag{5}$$

where α is the absorption coefficient, E_g is the energy band gap, $h\upsilon$ is the incident photon energy and A is a constant dependent on the effective masses of the electron and the hole and the material refractive index.

Figure 12 shows the variation of $(\alpha h\upsilon)^2$ versus $h\upsilon$ for the three samples.

The direct band gaps are estimated to be 1.50, 1.52 and 1.53 eV for samples S0, S20 and S70, respectively. The above values obtained for CdTe polycrystalline films are in good agreement with the reported value of 1.514 eV at room temperature for a CdTe single crystal [35] as well as the reported value of 1.50 eV for CdTe thin films [36, 37].

The refractive index (n) of the specimens was calculated using the following equation [17]:

$$n = \frac{\left[(1+R) + \{(1+R)^2 - (1-R)^2(1+k^2)\} \times 1/2\right]}{1-R}, \tag{6}$$

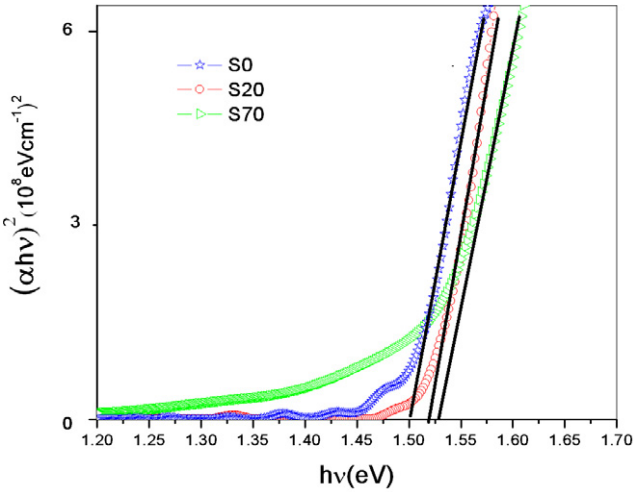

Figure 12. Variation of $(\alpha h\upsilon)^2$ versus $h\upsilon$ (photon energy) for the three samples.

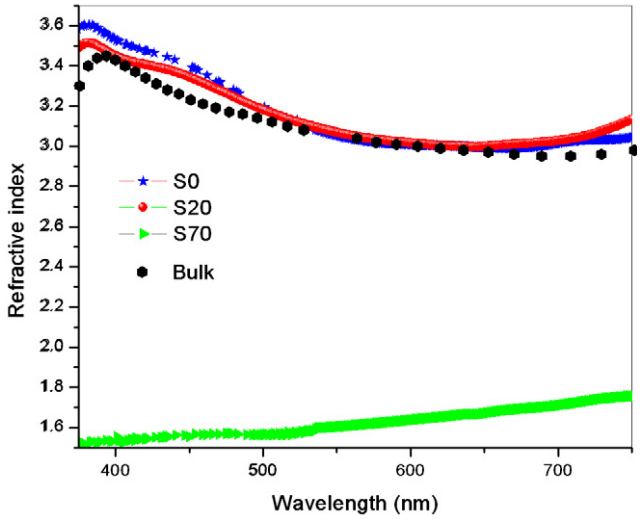

Figure 13. Variation of refractive index (n) with incident photon energy $h\upsilon$ in the samples.

where R is the reflection coefficient, $k = (\alpha\lambda)/4\pi$, and α and λ are the absorption coefficient and light wavelength, respectively.

Using equation (6) the variation of refractive index (n) for all the samples was obtained and is shown in figure 13. It is observed that the refractive index decreases as the vapor flux angle increases. For comparison, the refractive index of bulk CdTe as a function of wavelength, supplied by the Sopra Material Database (www.sopra-sa.com), has been presented in the figure. The refractive index values of S0 and S20 are close to that of bulk CdTe material while that of S70 is considerably lower. The same observation has been reported by others for obliquely deposited films [18–21, 26]. The physical interpretation of the decrease in the refractive index of the nanostructure sample (S70) can be described by its high porosity. Due to the porosity in GLAD films, the effective refractive index should be a combination of the refractive indices of the film material and air [38]:

$$n_{\text{eff}} = n_0 \frac{\rho}{\rho_0} + n_{\text{air}} \left(1 - \frac{\rho}{\rho_0}\right). \tag{7}$$

Substituting the ρ to ρ_0 ratio from equation (3) in the above equation, one can obtain a relation relating the effective refractive index to the incident flux angle:

$$n_{\text{eff}} = n_0 \frac{2\cos\alpha}{1+\cos\alpha} + n_{\text{air}} \left(1 - \frac{2\cos\alpha}{1+\cos\alpha}\right). \tag{8}$$

Using the above expression, the refractive index of S70 was calculated and found to be 2.02. This may be an interesting finding since using the GLAD method, one can control the refractive index of films for optical applications. The difference between the calculated refractive index value of S70 and the average one corresponding to the curve shown in figure 13 may be attributed to the structural phase transition observed in this sample.

4. Conclusions

Cadmium telluride films have been prepared by the GLAD technique with different incident vapor flux angles, namely 0°, 20° and 70°. Using the XRD patterns, the samples were found to be polycrystalline with cubic structure, except for the one prepared at high vapor flux angle that showed hexagonal structure. The FESEM image of S70 revealed its porous nanocolumnar structure. The optical studies showed that the energy band gap value of all the samples was close to that of CdTe single crystals, which is an indication of their good degree of crystallinity. A higher absorption coefficient in the visible and near-IR spectral range has been observed for S70. This is a very important result because for photovoltaic applications, absorber materials having large absorption coefficients are needed. Also, due to the existence of porosity in the nanostructure sample, the refractive index decreased considerably.

References

[1] Thornton J A 1974 *J. Vac. Sci. Technol.* **11** 666
[2] Massier R, Giri A P and Roy R A 1984 *J. Vac. Sci. Technol.* A **2** 500
[3] Kelly P J and Arnell R D 1998 *J. Vac. Sci. Technol.* A **16** 2858
[4] Barma P and Aduamik M 1998 *Thin Solid Films* **317** 27
[5] Robbie K and Brett M J 1997 *J. Vac. Sci. Technol.* A **15** 1460
[6] Hawkey M M and Brett M J 2007 *J. Vac. Sci. Technol.* A **25** 1317
[7] Knorr T G and Hoffman R W 1959 *Phys. Rev.* **113** 1039
[8] Driks A G and Leamy H J 1977 *Thin Solid Films* **47** 219
[9] Tait R N, Smy T and Brett M J 1993 *Thin Solid Films* **226** 196
[10] Xiao X, Dong G, Shao J, He H and Fan Z 2010 *Appl. Surf. Sci.* **256** 1636
[11] Robbie K and Brett M J 1996 *Nature* **383** 616
[12] Suzuki M and Taga Y 1992 *J. Appl. Phys.* **71** 2848
[13] Malac M and Egerton R F 2001 *J. Vac. Sci. Technol.* A **19** 158
[14] Lisfi A and Lodder J C 2001 *Phys. Rev.* B **63** 174441
[15] McMichael R D, Lee C G, Bonerich J E, Chen P J, Miller W and Egelhoff W F 2000 *J. Appl. Phys.* **88** 3561
[16] Hodgkinson I J, Wu Q H, Thorn K E, Lakhtakaia A and McCall M W 2000 *Opt. Commun.* **184** 57
[17] Al-Ghamdi A A, Khan S A, Nagt A and Abd Ei-Sadek M S 2010 *Opt. Laser Technol.* **42** 1181
[18] Xiao X, Dong G, Xu C, He H, QI H, Fan Z and Shao J 2008 *Appl. Surf. Sci.* **255** 2192

[19] Chaffar Akkari F, Kanzari M and Rezig B 2008 *Mater. Sci. Eng.* **28** 692
[20] Wang S, Xia G, Fu X, He H, Shao J and Fan Z 2007 *Thin Solid Films* **515** 3352
[21] Chaffar Akkari F, Kanzari M and Rezig B 2008 *Physica* E **40** 2577
[22] Sharma S K and Srivastava R S 1987 *J. Appl. Phys.* **62** 907
[23] Dhere N G, Pinherio R G and Parikh N R 1974 *J. Vac. Sci. Technol.* **11** 599
[24] Ehsani M H, Rezagholipour Dizaji H and Mirhaj M H 2012 *Dig. J. Nanomater. Biostruct.* **7** 629
[25] Sharnilova K V, Bulotov O S, Voronkov E N and Dimitriev V A 1966 *Sov. Phys.—Crystalloger.* **11** 431
[26] Wang S, Fu X, Xia G, Wan J, Shao J and Fan Z 2006 *Appl. Surf. Sci.* **252** 8734
[27] Singh S N and Kumar D 2008 *J. Appl. Phys.* **103** 023713
[28] Beach J D and McCandless B E 2007 *Mater. Res. Soc. Bull.* **32** 225
[29] Swanepoel R 1983 *J. Phys. E: Sci. Instrum.* **16** 1214
[30] Sanchez-Gonzalez J, Diaz-Parralejo A, Ortiz A L and Guiberteau F 2006 *Appl. Surf. Sci.* **252** 6013
[31] Ashour A, Kadry N E and Mahmoud S A 1995 *Thin Solid Films* **269** 117
[32] Wu X, Lai F, Lin L, Zhuang B, Yan Q and Huang Z 2008 *Appl. Surf. Sci.* **254** 6455
[33] Hädrich M, Metzener H, Reislöhner U and Kraft C 2011 *Sol. Energy Mater. Sol. Cell* **95** 887
[34] Pankove J I 1971 *Optical Processes in Semiconductors* (New York: Dover) p 34
[35] Yu Z, Hofer S G, Giles N C, Myers T H and Summers C J 1995 *Phys. Rev.* B **51** 13789
[36] Shaaban E R, Afify N and El-Taher A 2009 *J. Alloys Compounds* **482** 400
[37] Rakhshani A E 1997 *J. Appl. Phys.* **81** 7988
[38] Hu L, Wang P, Wan X and Jiang S 2012 *J. Mater. Sci. Technol.* **28** 97